CHAPTER 9

Borehole observations of continuous strain and fluid pressure

Evelyn A. Roeloffs and Alan T. Linde

Strain is expansion, contraction, or distortion of the volcanic edifice and surrounding crust. As a result of magma movement, volcanoes may undergo enormous strain prior to and during eruption. Global Positioning System (GPS) observations can in principle be used to determine strain by taking the difference between two nearby observations and dividing by the distance between them. Two GPS stations 1 km apart, each providing displacement information accurate to the nearest millimeter, could detect strain as small as 2 mm km^{-1}, or 2×10^{-6}. It is possible, however, to measure strains at least three orders of magnitude smaller using borehole strainmeters. In fact, it is even possible to measure strains as small as 10^{-8} using observations of groundwater levels in boreholes.

Since volcanic strain may be very large, techniques capable of detecting minute amounts of deformation might seem like overkill. There are, however, numerous advantages to high-resolution strain measurements for studying volcanic deformation. Their high sensitivity allows these instruments to be deployed farther from the volcano. Borehole strainmeters operate automatically, with little field maintenance to bring observers into danger, and can continue to transmit data throughout, and after, an eruption. High strain sensitivity is achieved without long observation periods, allowing sampling at up to 200 Hz. Detecting the tiny surface deformation resulting from magma movements at several kilometers depth provides information about the physics of volcanic eruptions, and as the examples will show, borehole strain and water level data enhance predictive capability because aseismic deformation can precede the onset of pre-eruptive volcanic seismicity.

In this chapter, we describe the design and capabilities of borehole strainmeters, as well as ways of interpreting water level measurements in terms of crustal strain. Data-analysis procedures are outlined. Finally, we summarize examples of strain and fluid-pressure changes recorded during volcanic unrest.

9.1 BOREHOLE STRAINMETER DESIGN AND CAPABILITIES

Detecting strain due to volcanic activity (or any tectonic activity) is challenging because the Earth's surface is an extremely noisy environment. Fortunately, large strain changes due primarily to weather and cultural effects diminish with depth below the surface. Tremendous improvements in the signal-to-noise ratio can be realized by installing sensors at depths of about 200 m below the surface. The most feasible and cost-effective way of achieving this is to install the sensor deep in a small-diameter (typically less than 15 cm) borehole.

The borehole installation is shown schematically in Figure 9.1. The highest quality data come from instruments installed below active aquifers and in competent rock. When the hole is complete, a quantity of expansive cement, or grout, is lowered in a container to the bottom of the hole. The container opens and is withdrawn, depositing the cement at the bottom in a way that avoids separation of sand and cement. The strainmeter is then lowered into the hole and sinks through the grout that completely surrounds and covers the instrument. As the grout hardens, it expands and locks the strainmeter to the surrounding rock. Because the strainmeter is

D. Dzurisin, *Volcano Deformation*

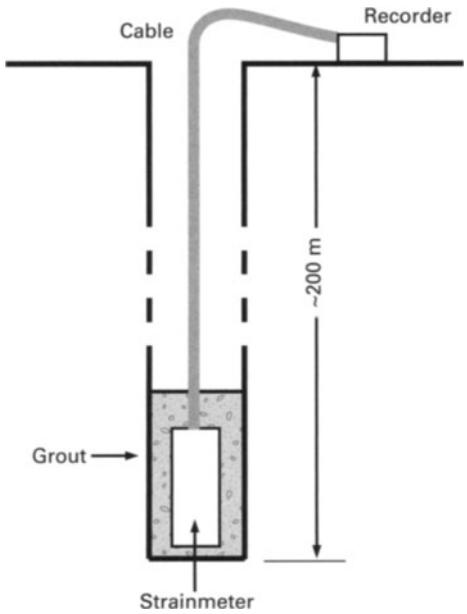

Figure 9.1. Schematic diagram of a borehole strainmeter installation.

resilient, it will then track subsequent deformation of the rock wall.

The borehole strainmeters that have so far provided almost all the strain data relating to volcanic activity have been Sacks–Evertson instruments, often referred to as 'dilatometers' (Sacks *et al.*, 1971). See Agnew (1986) for descriptions of other types of strain instrumentation. The strain-sensing chamber of the strainmeter (Figure 9.2) is a long (~3 m) cylindrical stainless steel cylinder (7 cm diameter) effectively filled with a liquid, typically silicone oil. Both horizontal and vertical strain modify this cylinder's volume, causing oil to move in or out of the volume. Attached to the sensing chamber is a small bellows (12.7 mm in diameter) whose length changes in proportion to the amount of oil entering or leaving the chamber. The position of the top of the bellows is measured by means of a differential-transformer-based displacement transducer (DT1) with a resolution of about 1 nanometer (1 nm = 10^{-9} m). The geometric ratio between the sensing unit and the bellows provides hydraulic amplification of about 40,000 and, since hydraulic amplifiers are effectively noise free, the instrument has a resolution of about 10^{-12} in strain. The bellows has limited extension capabilities (about 5 mm) so a hydraulic valve, controlled by surface electronics, is used to allow a reset of the sensing hydraulics. The dynamic range of the instrument is about 140 dB (more than a 24-bit analog-to-digital (A/D) converter). Since 1998 this

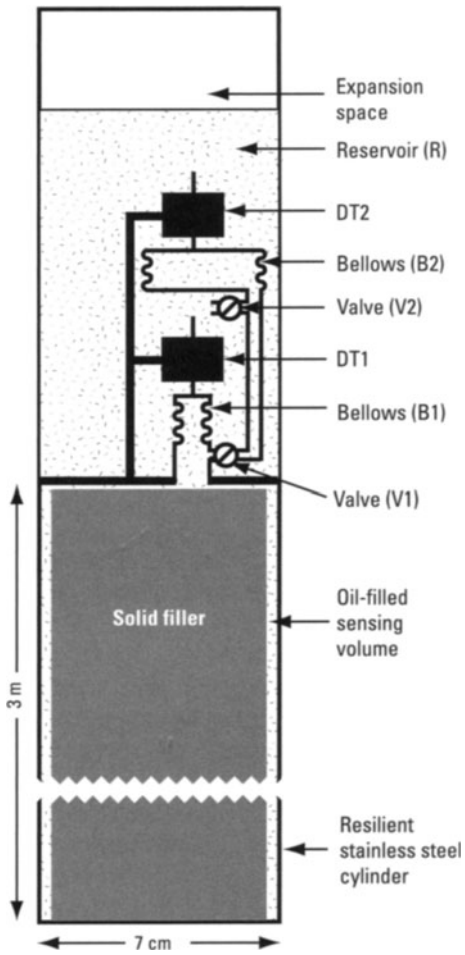

Figure 9.2. Diagram of a Sacks--Evertson two-stage borehole dilatometer; see text for discussion.

design has been modified to incorporate a second, less sensitive bellows-displacement transducer-valve assembly (DT2). The exit port of the primary valve is connected to a second, larger diameter (5 cm) bellows that is also monitored with a DT. A second valve allows this bellows to be equilibrated with an unstressed oil reservoir. No data are lost during the reset procedure since only one valve is open at a time. During normal operation, both valves are closed so that the second bellows responds to changes in volume of an unstressed constant mass of oil (i.e., the second DT2 output voltage is a measure of temperature changes with resolution better than 10^{-4} °C). The instrument is connected to surface electronics by a cable that provides power for the displacement transducers as well as the various signals.

The electronic unit provides a regulated voltage supply and monitors the output signals to implement opening and closing of the valves. The

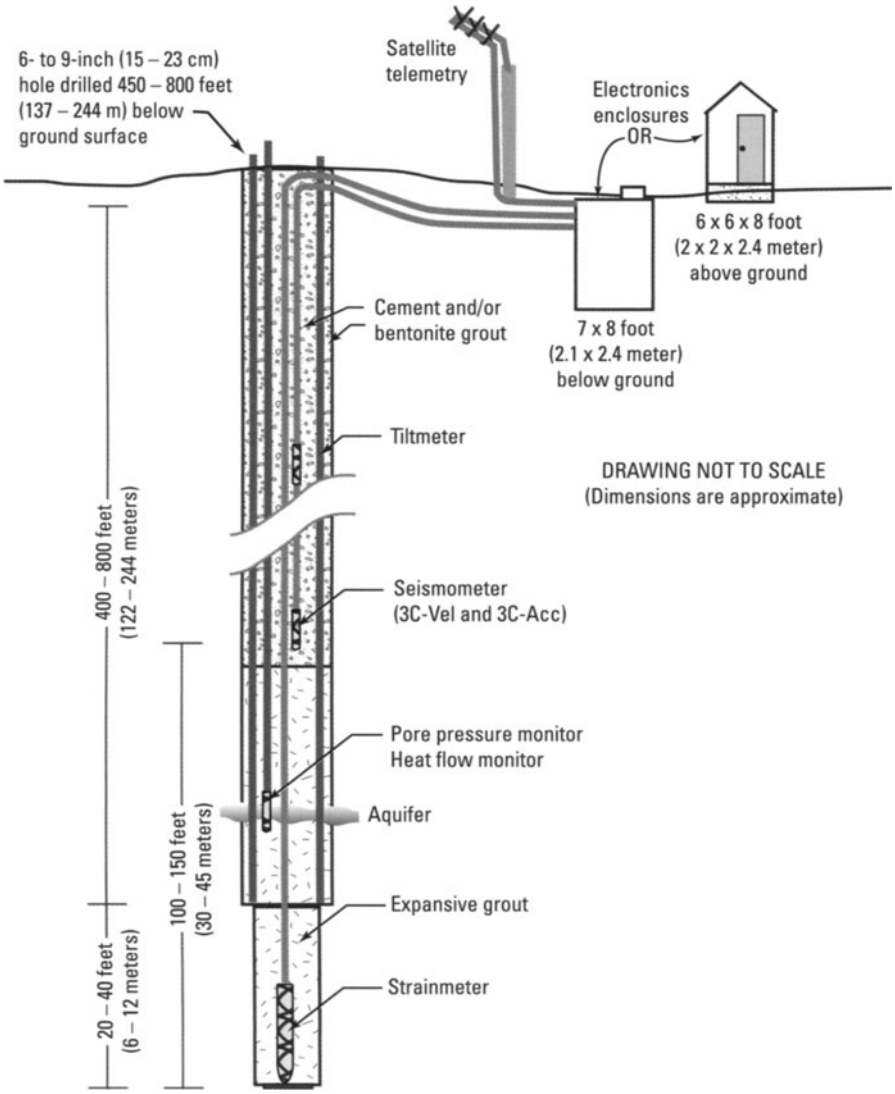

Figure 9.3. Schematic diagram showing a well-instrumented borehole-monitoring station, including a strainmeter, pore-pressure and heat-flow monitors, seismometer, tiltmeter, telemetry, and electronics enclosure.

displacement transducer output signals are analog voltages that are connected to A/D converters. Changes in atmospheric pressure also deform the near-surface rock, so it is necessary also to record barometric changes with resolution of at least 1 hectopascal (1 hPa = 1 millibar). An inexpensive GPS receiver is incorporated to provide absolute time information. The data can be recorded on site as well as transmitted to a central recording location. The total on-site power consumption is small enough that solar cells or wind generators are able to power remote installations. The strainmeter frequency response is flat from 0 Hz to more than 10 Hz so that sampling at about 50 times per second with 24-bit resolution is needed for complete recording of the instrument output.

Drilling suitable boreholes is relatively expensive and thus measures need to be taken to ensure that the data return more than justifies the initial expense. The majority of the borehole strainmeters installed during the last 15 years, using recommended procedures, are still operating, and some borehole strainmeters have been in continuous operation for more than 20 years. Strainmeter boreholes also provide very quiet sites for seismometers and, in many cases, downhole seismometers are installed with the strainmeters. Tiltmeters can be installed in the same holes and it is also possible to include sensing of pore pressure at depth. Thus, the borehole can provide a number of different data streams for a time period that is more than adequate to justify the costs. Figure 9.3 shows a scheme for installing all of these types of instruments in a single borehole. The

data obtained from such installations provide critical information for understanding volcanic activity.

Although each strainmeter can be calibrated before installation, in practice the instrument must be calibrated *in situ* by analyzing its response to Earth tides. The tidal calibration is necessary because the strainmeter output is a function of the elastic properties of the instrument as well as of the formation in which it is installed. Tidal calibration is usually accomplished by determining the amplitude of the M_2 tidal constituent in the strainmeter data and equating this to the calculated amplitude, computed from the site's latitude and longitude, with modifications for ocean loads. Software for estimating the amplitudes of tidal constituents from hourly data is described by Ishiguro (1981), and ocean load corrections can be computed using the program GOTIC2 described by Matsumoto *et al.* (2001). Earth-tidal variations recorded by strainmeters are generally closely in phase with calculated Earth-tidal strains, so that the strainmeter data can be expressed in terms of strain using only a multiplicative factor. Strainmeter data can usually be adequately corrected for atmospheric-pressure effects using a single coefficient of proportionality. The instrument output is proportional to a combination of areal and vertical strain. Since, compared with the tectonic sources being studied, the strainmeters are very close to the Earth's surface, it can be assumed that vertical stress vanishes, so that vertical and areal strain are proportional. Under this assumption, the relative weightings of strainmeter sensitivity to vertical versus areal strain are unimportant, and the instrument is thought of as measuring either areal or volumetric strain.

Borehole strainmeters yield very sensitive measurements of time variations in strain, but do not provide useful information about absolute strain rates. Although the strainmeter has constant response to strain changes over an extremely broad frequency band (0 Hz to >10 Hz), the data from a borehole site will generally be most reliable over a smaller band. Initial transients due to curing of the expansive grout (time constant of months) and to viscoelastic relaxation of stress around the newly drilled borehole (time constant typically of a year or more) perturb the record, albeit with removable exponential trends. Tectonic deformation at periods of several months may be masked by seasonal effects of precipitation and aquifer recharge, as well as possible instrument drift. At periods longer than about a year, the data may reflect instability of the geological environment in the immediate vicinity of the hole rather than signals of tectonic interest. Such noise characteristics can vary greatly at different sites and special care should be taken in the interpretation of signals in the seasonal period range and at very long periods. In general, however, the data are very reliable at periods less than a few months and may well provide important data at periods at least as long as a year after careful analysis in conjunction with other types of data.

During volcanic activity that involves magma movement, deformation around the volcano generally results from a compound source. To determine the characteristics of the sources (e.g., a deflating magma reservoir combined with a propagating dike), it is necessary to measure the strains at a number of sites around the volcano. Ideally, there would be sites covering all azimuths and at a variety of distances from the volcano, from about 2 km to several times the reservoir depth. Financial support and logistical considerations limit both the number of sites and where they can feasibly be located. Site selection is strongly influenced by knowledge of the geological structure because the best quality data come from strainmeters installed in competent rock. With a network of about 5 well-distributed borehole sites, the strain information can place strong constraints on source models. Since dilatational strain from subsurface magma chambers and dikes is a strong function of the source depth (undergoing a change in sign at distances dependent on that depth), continuous strain data allow upward dike propagation to be tracked with time, which has potential for the prediction of eruptions (see below).

9.2 GROUNDWATER LEVEL AS A VOLUMETRIC STRAIN INDICATOR

Crustal deformation can produce fluid-pressure fluctuations in subsurface formations. These pressure fluctuations can be measured directly in a borehole sealed from the atmosphere, but it is usually easier to measure groundwater level in an open well, which acts as a manometer. The variation in groundwater level Δh is related to the pressure variation Δp as $\Delta p = \rho g \Delta h$, where g is the acceleration due to gravity and ρ is the density of fluid. Here we will use the terms groundwater level and fluid-pressure change interchangeably.

Groundwater level variations in a borehole can be recorded using a pressure transducer suspended below the water surface in an open well. If feasible,

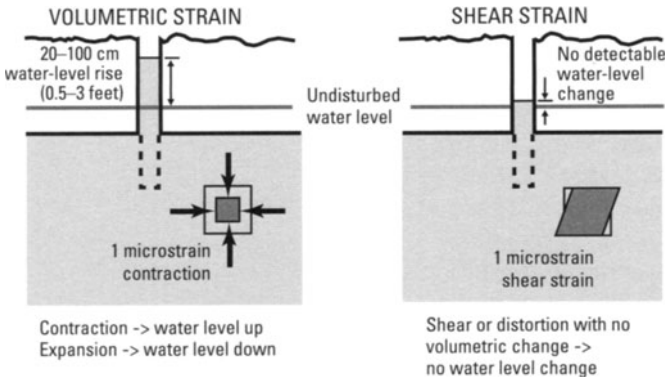

Figure 9.4. Diagram illustrating the water-level changes produced in a porous formation by volumetric strain as opposed to shear strain.

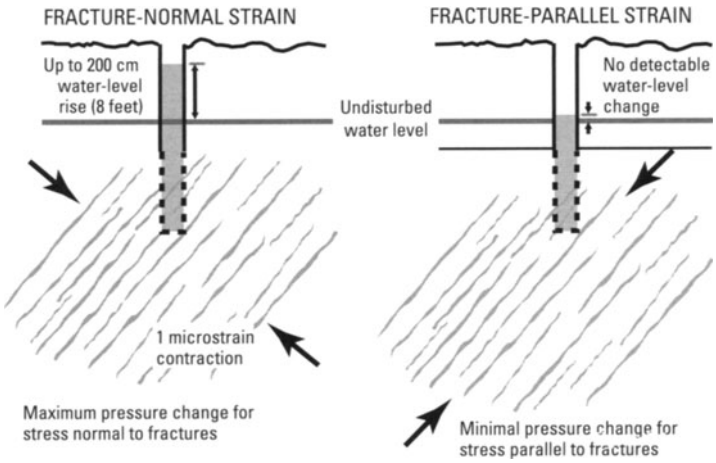

Figure 9.5. Diagram illustrating the water level response of a fracture-dominated formation to fracture–normal strain as opposed to fracture--parallel strain.

a device called a 'packer' can be installed to seal the fluid pressure from the atmosphere, in which case the transducer is placed below the packer, while a power and instrumentation cable passes through it. Compared with a borehole strainmeter, the transducer is many times less expensive, and in some cases existing boreholes or wells can be instrumented. The low cost and simplicity of the data collection, however, are offset by lower sensitivity to strain and greater complexity of data analysis. Like borehole strainmeters, groundwater level variations also are of limited value at long periods, with the upper limit of the period of usefulness sometimes difficult to determine. Nevertheless, water level observations have yielded some intriguing examples of pre-eruptive crustal deformation as well as crustal deformation accompanying earthquake swarms.

9.2.1 Water levels and crustal strain

Why should water levels in wells respond to crustal strain? The reason is that deforming a rock changes the volume of pore space, which in turn causes the pressure in the fluid to change. Such strain-induced changes generally dissipate with time due to fluid flow.

The ratio of water level change to strain depends critically on certain properties of the formation being monitored. For many rocks in which void space is distributed approximately uniformly in the form of pores, changes of pore volume occur primarily with rock deformation that changes the overall volume of the rock (Figure 9.4). That is, shear deformation with no associated volume change has little effect on groundwater level. For a rock in which void space is dominated by fractures with a preferred orientation, fluid pressure in the fractures is most greatly affected by deformation that is normal to the plane of the fractures (Figure 9.5). Other features that affect fluid-pressure response to strain are the elastic properties of the rock, and the degree of connection to the water table.

The mathematical formulation for the coupling between the elastic deformation of a porous rock

and the pressure of fluids in the pores was first developed by Biot (1956, 1941), with a useful revisiting by Rice and Cleary (1976). Wang (2000) provides a comprehensive summary. Of chief importance to understanding water level fluctuations caused by crustal deformation is that, in the absence of fluid flow, fluid-pressure changes are proportional to changes in average stress $\Delta\sigma_{kk}$ or, equivalently, in volumetric strain $\Delta\varepsilon_{kk}$ according to:

$$\Delta p = -B\Delta\sigma_{kk} = -(BK_u)\Delta\varepsilon_{kk} \qquad (9.1)$$

In (9.1), the minus signs are needed because pore pressure decreases with positive (extensional) stress or strain. B, known as Skempton's coefficient, is a dimensionless material property with a value between 0 and 1, and K_u is the porous material's undrained bulk modulus. There are few measurements of Skempton's coefficient from laboratory work, but those that exist confirm this range of values. Moreover, Skempton's coefficient and the undrained bulk modulus can also be inferred from other rock properties: rock bulk modulus, porosity, and fluid and grain compressibility. These calculations, observations of Earth tides in wells, and laboratory studies suggest that the coefficient of proportionality between water level changes and volumetric strain is in the range of 30–100 cm per microstrain (1 microstrain $= 10^{-6}$) for rocks whose void space is in the form of pores.

In a rock where void space is dominated by fractures, the sensitivity of water pressure to strain can be greater than in a porous rock, but is not as easily calculated based on rock properties because the coefficient depends on fracture compliance. Bower (1983) has shown how to relate fracture parameters to observed Earth tide response. Observed coefficients of water level change in response to strain in fracture-dominated formations are as high as 2 m per microstrain (e.g., Woodcock and Roeloffs, 1996).

Fluid pressure changes in wells that respond to Earth tides can be expressed in units of strain by the same technique used for calibrating borehole strainmeters. In water level data, however, tidal variations may lead or lag actual tidal strain due to time-dependent flow in the well–aquifer system (Roeloffs, 1996). Poorly confined aquifers may also have frequency-dependent responses to atmospheric pressure (Rojstaczer, 1988; Rojstaczer and Agnew, 1989). If these effects are significant, then they can be taken into account in converting water level measurements to units of strain.

9.2.2 Effects of groundwater flow

Subsurface fluid pressure of course also varies in response to rainfall, pumping, or any other factor changing the mass of fluid in the system. When fluid mass per unit volume of material is not constant, (9.1) generalizes to:

$$\Delta p = BK_u - \Delta\varepsilon_{kk} + \left[\frac{1}{1 - K/K_s}\frac{m - m_0}{\rho_0}\right] \qquad (9.2)$$

where K is the (drained) bulk modulus of the material, K_s is the bulk modulus of the solid grains, and $(m - m_0)/\rho_0$ is the change in fluid mass per unit volume, divided by the fluid density in a reference state. Equation (9.2) shows that fluid mass changes are coupled not only to fluid pressure changes, but also to volumetric strain changes. One implication of this coupling is that when measurements of strain exhibit time variations, it is generally necessary to evaluate climatic or artificial changes in subsurface fluid pressure as a causative factor rather than attributing the deformation to tectonic causes.

Fluid pressure changes in response to strain occur instantaneously with deformation. In fact, the water level variation would have the same time history as the deformation were it not for the ability of water to flow. Flow causes spatial variations in pressure to equilibrate with each other over a timescale governed by the material's hydraulic diffusivity. In particular, a sudden, localized change of pore pressure induced by a tectonic event such as an earthquake or rapid intrusion will spread and dissipate with time, causing time-dependent fluid pressure changes in locations not originally affected by the tectonic event. Although in principle the pore pressure field is always coupled to elastic deformation, in practice the time-dependent fluid pressure field can often be adequately modeled using a groundwater model that solves the (uncoupled) diffusion equation of groundwater flow.

An important factor that limits the usefulness of water level monitoring is the flow path from the depth where pressure is sensed to the water table (Figure 9.6). When strain is applied far below the water table, the pressure in the fluid changes because the volume available for it to occupy has changed. The strain may also affect the rock at the depth of the water table. However, at the water table, fluid has the option of moving up or down into unoccupied pore space. There is a very large difference between the amount by which the water table must change, and the equivalent pressure head induced by a pressure change at depth. For example, a water pressure

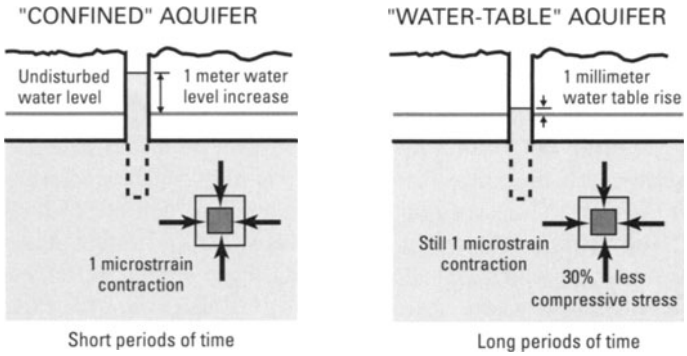

Figure 9.6. Diagram illustrating the greater response of fluid pressure to strain in a confined aquifer as compared with a water table aquifer.

rise of 0.01 MPa (1.45 psi) increases the water level in a well by 1 m. But the compressibility of water is 0.435 GPa^{-1}, so a fluid volume decrease of only 0.000 44% can relieve the pressure increase, if fluid can escape from the system. In a 100 m thick aquifer with 10% porosity, removal of 0.000044 cubic meters from each 1-m square area of aquifer would relieve the pressure increase while causing a barely detectable water table drop of only 0.44 mm. Thus, if the strain is applied instantaneously, and remains in force, then the fluid pressure at depth will instantaneously change, while that at the water table will not. Upward or downward flow will occur in response to this induced gradient, with the time to equilibrate increasing as the square of the depth of measurement below the water table, and decreasing in inverse proportion to the hydraulic diffusivity. Since hydraulic diffusivity varies over many orders of magnitude, this timescale also varies tremendously. Figure 9.7 shows co-seismic water level changes at two different depths in the same borehole that recover at different rates due to the greater thickness of material over the deeper sensor. Figure 9.8 shows the range of times over which strain-induced pressure would be expected to persist. This range of timescales is one basis for distinguishing 'confined' from 'unconfined' aquifers, for purposes of characterizing their responses to strain. Although there is no specific cut-off point, a well in which a pressure disturbance caused by strain can persist for a month can usefully be thought of as 'confined', while a well in which a pressure disturbance caused by strain equilibrates within a matter of hours is behaving like an unconfined aquifer and is unlikely to provide useful information about tectonic strain. To achieve a sufficient degree of confinement, the observation well needs to be open to the formation at some depth below the water table, ideally 100 m or more. Aquifer pumping or slug tests (e.g., Moench, 1985) can be used to determine the hydrologic properties of monitoring wells, and in some

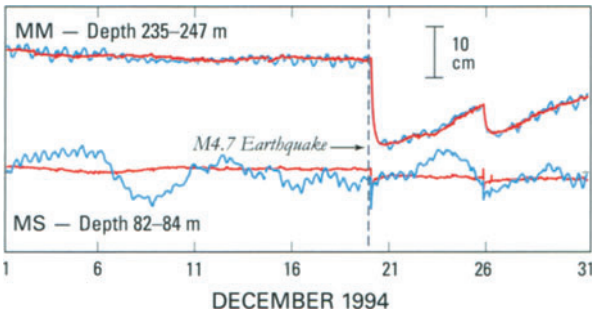

Figure 9.7. Raw (blue) and filtered (red) water level records from different depths in the Middle Mountain well near Parkfield, California, showing water level drops caused by a *M* 4.7 earthquake. Note rapid recovery in shallow interval (MS) and more sustained pressure change in deeper interval (MM).

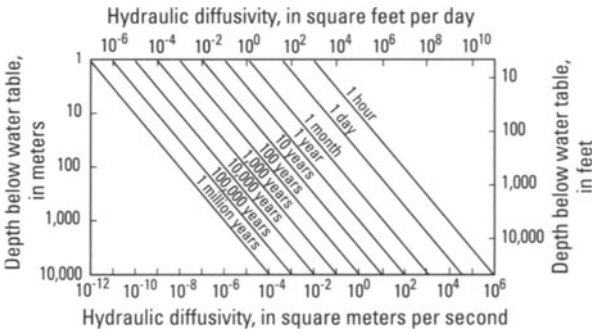

Figure 9.8. Range of times over which strain-induced pressure would be expected to persist, as a function of depth beneath the water table and vertical hydraulic diffusivity. The graph can be viewed as giving the elapsed time after the imposition of a strain step such that the response has fallen to one-tenth of its initial value. Modified from Roeloffs (1996).

cases can provide information on the connection between the monitored formation and the water table.

Segall *et al.* (2003) have shown that fluid flow can be expected to modify the output of a borehole strainmeter, if the strain varies with time at a rate that is slow compared with the flow. More specifically, this effect could limit the response of strainmeters to low-frequency strain changes, if the strainmeter is installed in a formation where there is a high-diffusivity path to the water table.

9.2.3 Thermal pressurization

Where hot magma or magmatic gases are in proximity to pore fluid, the heated fluid will undergo thermal expansion that tends to increase fluid pressure (Delaney, 1982; Bonafede, 1990). Typical thermal expansion coefficients for water under hydrostatic pressure in a region with a normal geothermal gradient range from $1.7 \times 10^{-4} {}^{\circ}\mathrm{K}^{-1}$ at 0.1 km depth to $9.3 \times 10^{-4} {}^{\circ}\mathrm{K}^{-1}$ at 5 km depth (Delaney, 1982). Pressures induced by heating of pore fluid tend to dissipate by fluid flow, so high hydraulic diffusivity can work against thermally induced pressure. During periods of volcanic unrest, intrusions typically occur over timescales of hours to days, and are particularly effective at raising fluid pressures, because flow cannot proceed rapidly enough to dissipate them. Bonafede (1990) estimated that, assuming a spherical source and typical rock properties, the pore pressure field generated by a 10°C increase of source temperature is comparable with that induced by a 10 MPa increase in source pressure.

9.2.4 Data collection requirements

As the examples will show, some volcanic eruptions have been preceded or accompanied by extremely large water level variations that were observed without special equipment. The simplicity of these observations is appealing and unequivocally demonstrates that groundwater levels change in response to volcanic deformation. Much more can be learned, however, from high-resolution water level measurements in well-characterized aquifers.

Water level data that are to be analyzed for tidal and barometric response need to be collected using sensors with a resolution of 1 mm of water or better. If the ratio of water level change to strain is 100 cm per microstrain, then sensor resolution of 1 mm corresponds to strain resolution of 1 nanostrain (1 nanostrain $= 10^{-9}$). In practice, the smallest strains that can be observed in water level data are about 10 nanostrain. The same pressure resolution is required for the barometric data as for the water level data, but in a network of closely spaced sites, it may not be necessary to operate a separate barometer at each site. Hourly data are ideal for tidal analysis, but more frequent sampling is helpful for detecting co-seismic water level changes. Most pressure transducers are prone to long-term drift, so it is worth visiting the site periodically to make manual measurements of water levels with a steel tape. Submersible pressure transducers are available to measure either absolute pressure, or pressure relative to the atmosphere (called a 'gauge' or 'vented' transducer). Either type of transducer can be used provided a stable, high-resolution barometer is available to allow the atmospheric pressure correction. An advantage of vented transducers is that an instrument with a smaller overall range can be used, since atmospheric pressure is not included in this range. However, special attention must be paid to preventing moisture from entering the vent tubes of such sensors and destroying the transducer. Meticulous splicing, storage in a dry environment, and maintenance of a desiccant pack over the vent tube's surface termination are required to avoid problems.

Water levels respond to rainfall and aquifer recharge. To date, the ability to model aquifer response to precipitation is limited, but nevertheless it is critical to make adequate measurements of precipitation. A well with a high sensitivity to strain can exhibit small water level changes due to the weight of heavy rainfall or snow accumulation on the Earth's surface. Aquifer pressure can usually be expected to change slowly in response to variations in the rate of rainfall, or, more generally, in the rate of surface infiltration. On or near a volcano, where weather varies dramatically with elevation, it is especially important to have nearby precipitation sensors and to be able to distinguish snow from rain in the data record. Daily records of precipitation are adequate for most purposes, but at remote sites a heated rain gauge sampled at the same interval as the water level sensors is ideal.

9.3 PROCESSING AND ANALYZING CONTINUOUS STRAIN AND WATER LEVEL DATA

Continuous deformation time series – strain or water level – accumulate at typical sampling

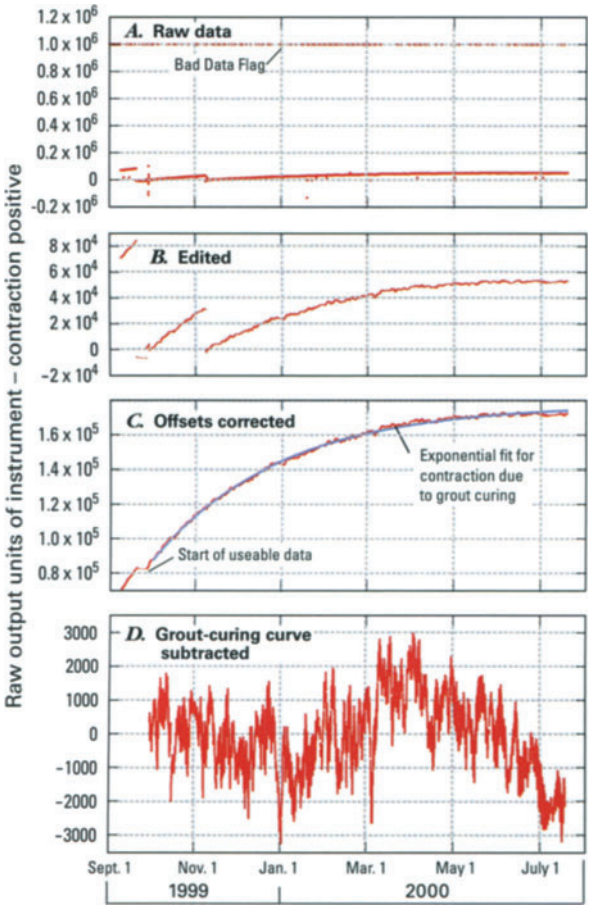

Figure 9.9. The first year of data from the Big Springs dilatometer at Long Valley Caldera, California. (A) Raw data as obtained from incoming telemetry. (B) Data with outliers removed. (C) Data corrected for offsets due to valve resets, with exponential curve fit superimposed. (D) Data after removal of exponential curve to account for contraction due to grout curing; see text for details. Data source: USGS Menlo Park.

intervals of minutes to an hour. The basic procedures for analyzing continuous deformation data are similar for strain, water level, and high-resolution tiltmeters.

Figure 9.9 illustrates these procedures using data from the Big Springs dilatometer, installed during the summer of 1999 on the north rim of the Long Valley Caldera in eastern California. Figure 9.9(A) shows the raw data as downloaded directly from incoming telemetry. A large number of points are equal to the 'bad' data flag 999999, and there are many additional outliers. Figure 9.9(B) shows the same dataset on an expanded scale after all outliers have been identified and replaced with the bad data flag. Large offsets in the first three months of the record are due to valve openings that bring the instrument back into range as it is compressed by curing of the expansive grout. In Figure 9.9(C), these offsets have been corrected for, resulting in a smoothly rising curve, except for a short initial period when field adjustments were being made. Figure 9.9(C) also shows a curve of the form $A_1 + A_2 \exp[C(t - t_0)]$, which was fit to the daily averages of the strain values to approximate the contraction imposed by the curing grout. In Figure 9.9(D), the data record is shown after subtracting the grout-curing curve. This time series now displays, among other possible signals, the strain variations due to tectonic processes, but it no longer contains absolute strain rate information. Comparing the 25-fold differences in the spans of the y-axes in Figures 9.9(C) and (D) underscores a fundamental feature of borehole–strainmeter data: because the instrument has such high resolution, it is not possible to discern all signals of tectonic interest until instrument resets and grout-curing effects have been removed from the data.

Figure 9.10 shows one month of data from the Big Springs dilatometer after removing strains due to Earth tides and atmospheric pressure loading; an

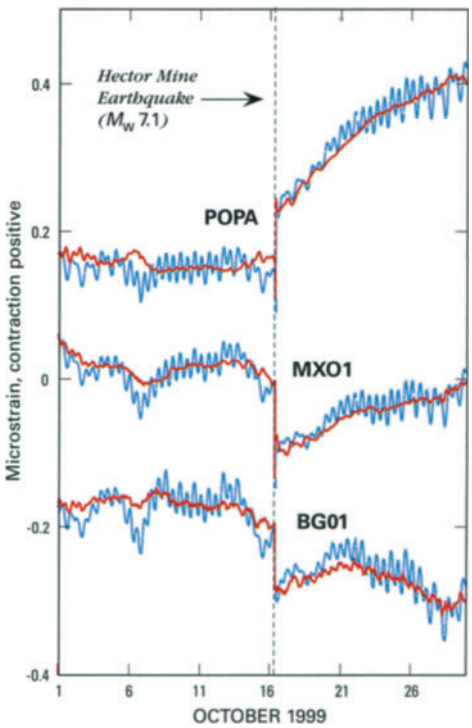

Figure 9.10. Strainmeter data from 3 Long Valley strainmeters, showing offset associated with the 16 October 1999, Hector Mine, California, earthquake (M_w 7.1, 416 km from Long Valley Caldera). Blue curves show data after editing, offsetting, and removal of long-term trend; red curves show data after removing effects of Earth tide and atmospheric pressure using harmonic analysis and linear regression.

offset due to the M_w 7.1 Hector Mine earthquake is well recorded. The tidal analysis also yields calibration factors that can be used to convert the strainmeter output to approximate units of strain.

The data may contain variations that are nontectonic in origin. Rainfall can affect water level observations by infiltration to the aquifer. For strainmeters and wells with high strain sensitivity, however, it is more common to record strain caused by the weight of the rain falling on the Earth's surface. Strain and water level variations induced by rainfall may be removed, but most commonly are left in the data and merely identified by comparison with a nearby record of rainfall.

Seasonal signals may also appear in both water level and strain data. Subsurface fluid pressure is known to vary seasonally in response to seasonal changes in the rates of rainfall and/or evapotranspiration. Strainmeter data are affected by the coupling between these fluid pressure changes and deformation, as well as by the weight of precipitation or snow on the Earth's surface. These effects can be difficult to model, so it is important to use caution in ascribing tectonic significance to seasonal changes in strain or fluid pressure.

9.4 VOLUMETRIC STRAIN FIELDS OF IDEALIZED VOLCANIC SOURCES

Mathematically, strain is a dimensionless tensor obtained by differentiating the displacement vector with respect to each coordinate direction (Chapter 8). In this section we describe the volumetric strain fields of a center of dilatation, a closed cylindrical source, and a vertical dike, all for the case of a homogeneous, isotropic elastic half-space with Poisson's ratio ν and shear modulus G.

9.4.1 Center of dilatation

The surface uplift due to a spherical cavity with a prescribed internal pressure change ΔP is the mathematical solution used most frequently to model measured volcanic displacements (Figure 9.11). Davis (1986) gives the expressions for the horizontal and vertical surface displacements, as well as a brief history of the solution. The solution is nominally only valid for a cavity whose radius a is much smaller than its depth d, but McTigue (1987) has shown that a more exact solution differs little. The common term 'Mogi' source refers to this solution with the Lamé constants equal (i.e., $\nu = 0.25$).

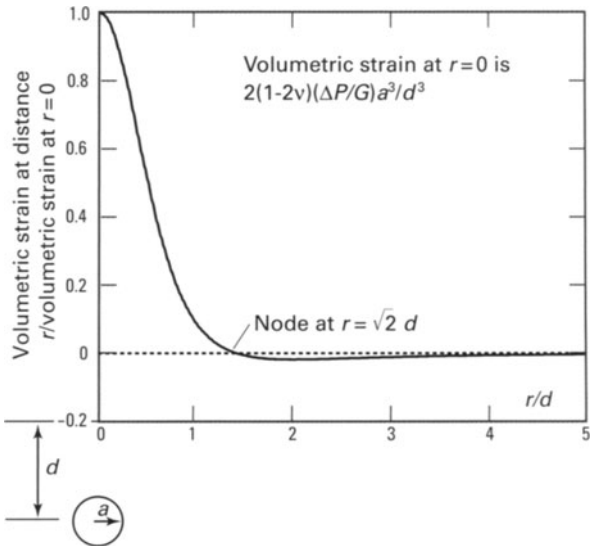

Figure 9.11. Diagram showing assumed configuration of a subsurface inflation source (center of dilatation), and plot of normalized volumetric strain versus dimensionless distance. See text for discussion.

The volumetric strain at the surface can be obtained by differentiating the radial displacement u_r (Equation 1a of Davis (1986)) to obtain $\varepsilon_{rr} = \partial u_r/\partial r$ and $\varepsilon_{\theta\theta} = u_r/r$. These two strain components are sufficient to obtain volumetric strain because at the free surface, the vertical stress must vanish, allowing the vertical strain ε_{zz} to be expressed in terms of the horizontal strains as:

$$\varepsilon_{zz} = -\frac{\nu}{1-\nu}(\varepsilon_{rr} + \varepsilon_{\theta\theta}) \tag{9.3}$$

The result is:

$$\varepsilon_{kk} = (1-2\nu)\frac{\Delta P}{G}a^3\frac{2}{(r^2+d^2)^{3/2}} - \frac{3r^2}{(r^2+d^2)^{5/2}} \tag{9.4}$$

Equation (9.4) is plotted in Figure 9.11 in nondimensional form. Like the solution for the displacements, the volumetric strain field is proportional to the ratio of pressure change to the shear modulus of the half-space. The largest strain changes are directly above the source, and are extensional when source pressure increases. Unlike the displacement field, however, the strain field changes sign at $r = \sqrt{2}d$. Beyond this distance, the greatest contractional value is approximately 2% of the maximum strain and occurs at a distance equal to twice the source depth. In practice, only two parameters can be

obtained by fitting (9.4) to a set of strain observations: the source depth and an estimate of $(1-2\nu)(\Delta P/G)a^3$, the source-volume change. If there is independent information about the size of the source and the elastic constants, then an estimate of the pressure change can be made. Alternatively, the coefficient can be expressed in terms of the volume change ΔV of the source by assuming that:

$$\Delta P = \frac{2G(1+\nu)}{3(1-2\nu)}\frac{\Delta V}{V} \tag{9.5}$$

Combining (9.5) with $V = (4/3)\pi a^3$ leads to the following alternate form of (9.4):

$$\varepsilon_{kk} = 0.5(1+\nu)\frac{\Delta V}{\pi}\frac{2}{(r^2+d^2)^{3/2}} - \frac{3r^2}{(r^2+d^2)^{5/2}}. \tag{9.6}$$

For a concrete example, consider the signals that might have been recorded had continuous strain instruments been in place at the time of the 1980 eruption of Mount St. Helens. Scandone and Malone (1985) infer that the magma chamber at Mount St. Helens is located at a depth of about 9 km (Figure 9.12), and that approximately 0.2 km^3 of material was erupted on 18 May 1980.[1] Assuming a spherical source geometry, a borehole strainmeter installed 18 km from the summit would likely have survived the eruption and would have recorded a contractional signal of about 1 microstrain.

The strain field for the center of dilatation can also be computed using the equations or computer code given by Okada (1992).

9.4.2 Vertical conduit models

Bonaccorso and Davis (1999) present analytic expressions for the surface displacements and tilts due to inflation of narrow vertical pipes. These models can be applied to situations where a narrow conduit connects a subsurface magma chamber to the surface or where the magma chamber itself is elongated in the vertical direction. The strains can be obtained by differentiating the published expressions numerically, or by symbolically differentiating them using software such as Mathematica.

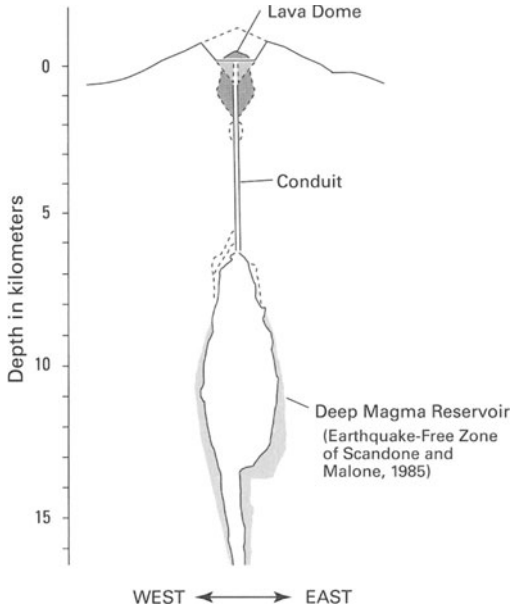

Figure 9.12. Cross-sectional view of Mount St. Helens, showing inferred locations and shapes of shallow- and deep-magma reservoirs.

The difference between the volumetric strain fields of the closed pipe source and the center of dilatation is most pronounced for radial distances less than one-half the source depth. The closed pipe source has maximum strain at about this radial distance, with smaller strain closer to the source. As an example, consider a more realistic vertically elongated model of the deep magma reservoir at Mount St. Helens (Figure 9.12), based on the zone observed by Scandone and Malone (1985) to have been devoid of earthquakes during the 1980 eruptions. Figure 9.13 shows volumetric strain from an assumed pressure change of 100 MPa, corresponding to about 10% of the pressure change in the main 1980 eruption. For both models, strains readily measured by borehole strainmeters would be expected within 10 km of the volcano, although distinguishing between these two reservoir geometries would clearly require more than one instrument. Periods of increased seismicity at Mount St. Helens since eruptive activity stopped in 1986

[1] The 9-km depth estimate is based on a model of surface-deformation data for June–November 1980, which show cumulative subsidence associated with five lesser explosive eruptions that followed the paroxysmal event of 18 May 1980. On that basis, plus the distribution earthquake hypocenters associated with the eruptions, Scandone and Malone (1985) proposed a model in which 1980 magma was supplied from depths of 7–14 km. According to the model, a mean source depth of 7 km would correspond to a source-volume change of 0.15 km^3, while a mean depth of 9 km would correspond to a source-volume change of 0.24 km^3 (Scandone and Malone, 1985, p. 254). The net volume of products erupted during the 6 explosive eruptions between 18 May 1980, and 16 October 1980, was estimated to be about 0.23 km^3, including 0.19 km^3 on 18 May (Scandone and Malone, 1985, p. 241, reporting values from Lipman *et al.*, 1981b).

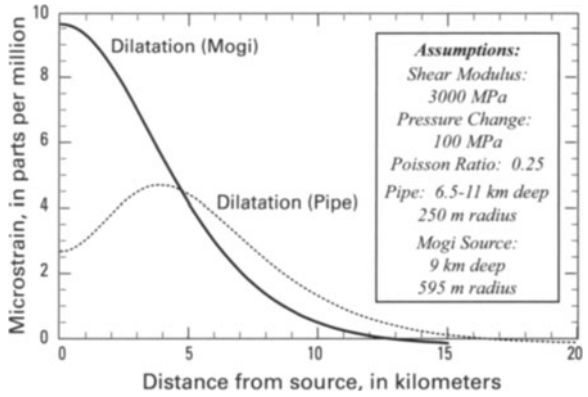

Figure 9.13. Volumetric strain fields from a pressure change in the deep magma reservoir under Mount St. Helens, assuming either a spherical (Mogi, 1958) or closed-pipe (Bonaccorso and Davis, 1999) geometry.

could reflect pressure changes in the deep reservoir (Moran, 1994), and these might produce deformation that would be detectable with borehole strainmeters.

9.4.3 Dike intrusion

The strain field of an inflating dike can be modeled as an opening-mode rectangular dislocation in an elastic half-space using the codes of Okada (1992). Figure 9.14 shows an example for a dike that is 5 km long and extends from 5 to 10 km beneath the surface. An interesting feature of the dike's strain field is the area of contraction directly over the dike. This feature, which is not present for a dike that reaches the surface, is surrounded by an area of extension. Unlike the center of dilatation or the closed cylindrical pipe, the maximum contraction produced by the dike is almost as great as the maximum extension. The width of the area of contraction decreases as the upper limit of the dike nears the surface; a strainmeter placed in this area of contraction will record a reversal in the strain field if the dike propagates far enough upward. To simulate strain from a propagating dike, the strain field can simply be calculated for a succession of positions of the source. To simulate the pore-pressure field of a propagating source is somewhat more complicated because the diffusing pressure fields must also be superimposed. Elsworth and Voight (1992) present a partially analytic solution in a moving coordinate system for pore pressure induced by advance of a dike intruding at a steady rate into a full space. They show that the solution closely resembles time-dependent pore-pressure changes recorded in a well several

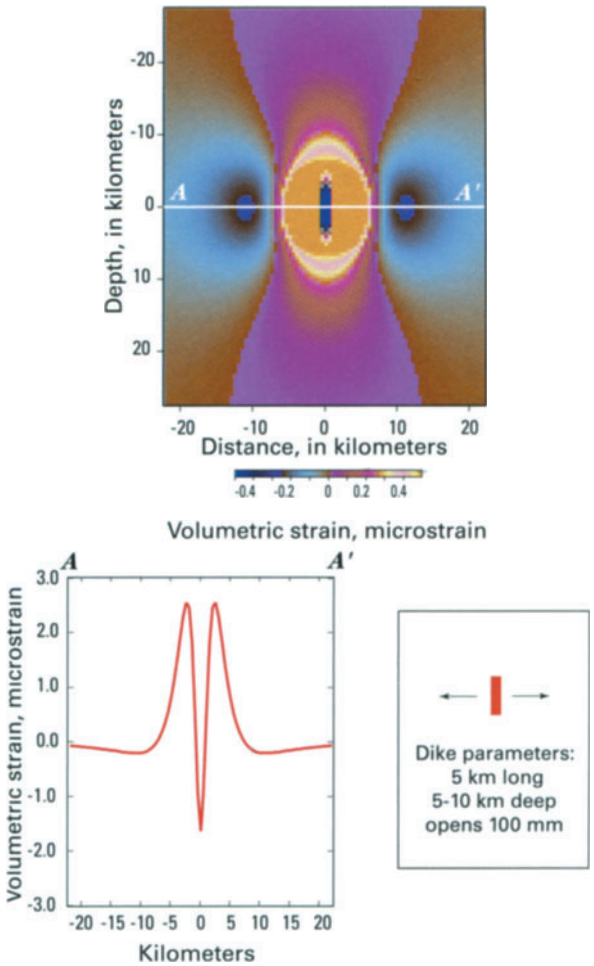

Figure 9.14. Volumetric strain field of a vertical dike, calculated using the computer code of Okada (1992).

kilometers from two dike intrusion events in Krafla, Iceland, in 1977 and 1978.

9.5 EXAMPLES

Water level changes preceding eruptions have on occasion been so large that they have been observed without special instrumentation. Newhall *et al.* (2001) review numerous examples of groundwater level changes associated with volcanic unrest and eruptions. For example, groundwater levels in wells on the upper slopes of Mayon Volcano, the Philippines, dropped as much as 2–3 m beginning several months before an eruption in 1993. These water level drops were attributed at least in part to inflation of the volcano accompanying subsurface upward movement of magma. Continuous water level data are now being collected to infer the magnitude

of the extensional strain and help constrain the influence of rainfall on the observations.

Below we discuss case histories for which actual strain and fluid pressure data have been recorded. Currently, there are detailed strain datasets for two eruptions of Hekla Volcano in Iceland and fluid pressure datasets for an eruption of Mount Usu in Japan. Crustal deformation was measured prior to all three of these eruptions. In addition, these sensitive techniques have detected crustal deformation accompanying earthquake swarms on the Izu Peninsula in Japan, on the Juan de Fuca Ridge in the western Pacific Ocean, and in the Long Valley Caldera, California. These deformation records strongly support the hypothesis that earthquake swarms in volcanic areas are a manifestation of the dominantly aseismic upward movement of magma in the form of dikes, which may or may not breach the surface to pose eruptive hazards.

9.5.1 Izu Peninsula, Japan

The Izu Peninsula in Japan is a volcanic area with ongoing uplift and frequent seismic swarms (Okada and Yamamoto, 1991). A submarine eruption off Ito City in 1989 was preceded by earthquake swarms and rapid strain and tilt, as well as groundwater outflow at four wells in Ito City, two of which have been monitored continuously since then. The strain, tilt, and deformation data from the 1989 eruption have been interpreted to indicate intrusion of subvertical dikes beneath a shear fault (Okada and Yamamoto, 1991). Between 1995 and 1998, several seismic swarms have been accompanied not only by water level changes (Ohno *et al.*, 1999; Koizumi *et al.*, 1999), but also by deformation recorded using borehole strainmeters, tiltmeters, and continuous GPS (CGPS). The water level changes accompanying the seismic swarms exceed those that would be expected in response to individual co-seismic strain steps due to swarm earthquakes. According to Ohno *et al.* (1999) and Koizumi *et al.* (1999), the sizes and directions of water level changes are consistent with their being proportional to the volumetric strain field calculated from the dike intrusion models.

9.5.2 Long Valley Caldera, California: stimulation by distant earthquakes

Groundwater levels in several wells, and discharges at several springs and creeks, have been monitored since the early 1980s at Long Valley Caldera, a potential volcanic hazard in eastern California. Tectonic and volcanic activity at Long Valley is monitored by a seismic network, periodic leveling surveys, a two-color electronic distance meter (EDM) network, three borehole volumetric strainmeters, a long-baseline tiltmeter, and, more recently, survey-mode and CGPS (Chapter 7). Although the volcano is judged unlikely to erupt anytime soon, it has exhibited a high rate of seismic activity and uplift in recent decades. Seismic swarms and accelerated uplift are closely watched, and local officials and the population are kept advised concerning volcanic hazards in case of renewed activity.

The intensive monitoring has revealed that local and distant earthquakes can induce persistent strain and water level changes at Long Valley that resemble those recorded during seismic swarms on the Izu Peninsula. The best-known example is the 1992 Landers, California, earthquake (M_w 7.3), whose effects in Long Valley, more then 400 km from the epicenter, included triggered microseismicity, a transient contractional signal on a borehole strainmeter, and water level changes (Hill *et al.*, 1995; Johnston *et al.*, 1995; Roeloffs *et al.*, 1995) (Figures 9.15 and 9.16). Other distant earthquakes that produced water level changes at Long Valley, but did not trigger seismicity, also have been

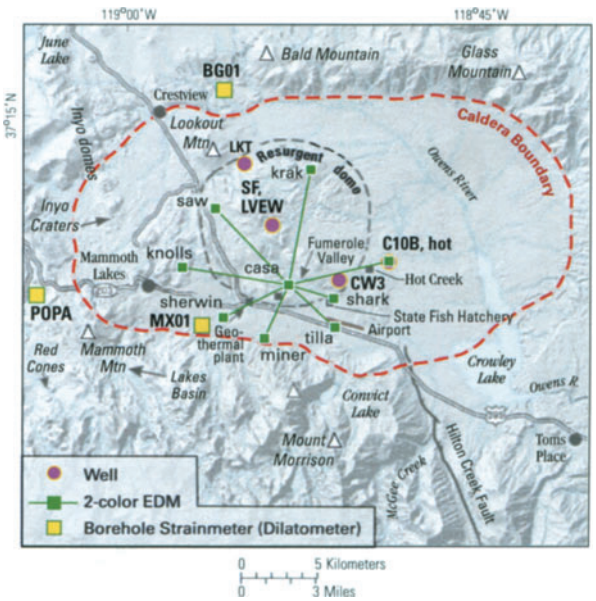

Figure 9.15. Map of the Long Valley Caldera area showing locations of the wells, strainmeters, and the two-color EDM network. The Hilton Creek Fault, Mammoth Mountain, and the resurgent dome are also shown.

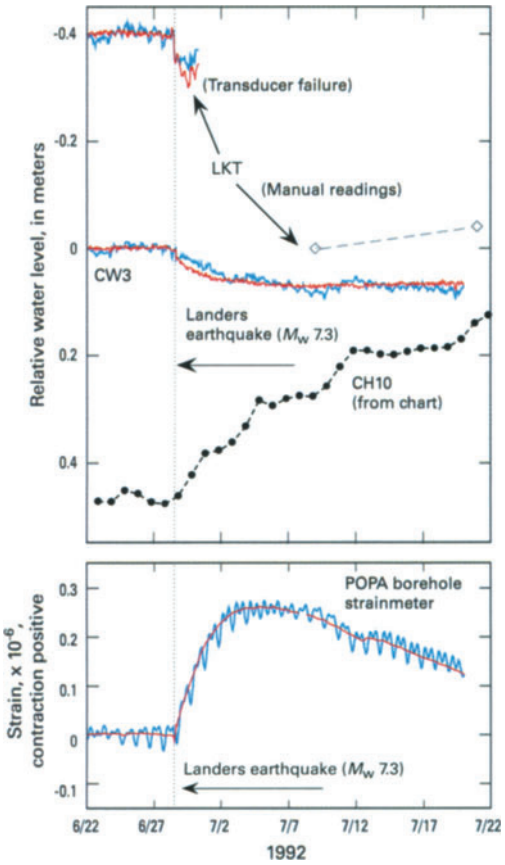

Figure 9.16. Earthquake-induced water level and strain changes at Long Valley Caldera caused by the 28 June 1992 Landers, California, earthquake (M_w 7.3), 446 km from Long Valley Caldera. Data with tidal and barometrically induced fluctuations removed (red) are superimposed on raw data (blue). A linear trend has been subtracted from the data so as to minimize the water-level variation in the 20 days before the earthquake.

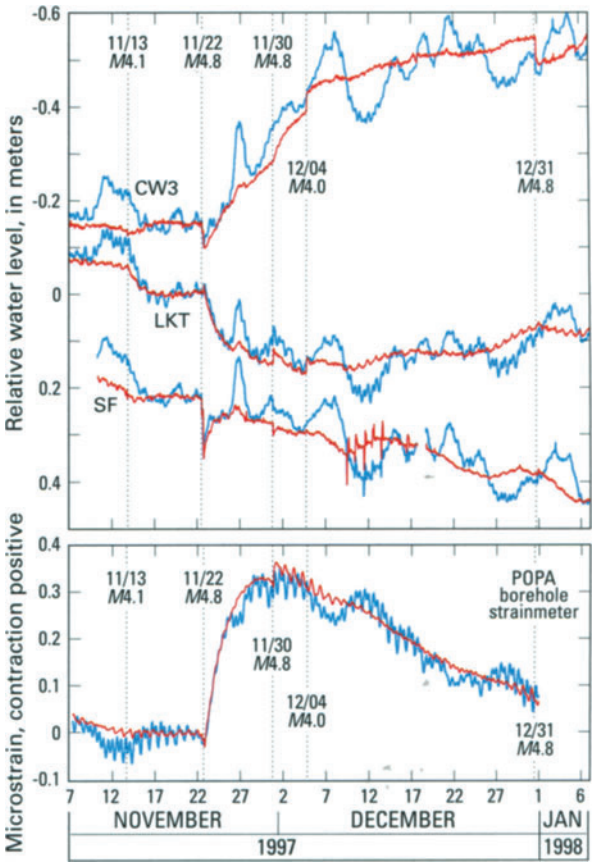

Figure 9.17. Earthquake-induced water level and strain changes at Long Valley associated with earthquakes in Long Valley Caldera, November–December 1997. Data with tidal and barometrically induced fluctuations removed (black) are superimposed on raw data (blue). A linear trend has been subtracted from the data so as to minimize the water level variation in the 20 days before the earthquake. Dotted lines mark occurrences of $M \geq 4$ earthquakes.

accompanied by strain-rate changes (Roeloffs *et al.*, 1998).

During an intensive earthquake swarm in late 1997, strain and water level changes closely resembling those induced by the Landers earthquake began simultaneously with one particular M 4.9 local earthquake on 22 November 1997 (Roeloffs *et al.*, 2003) (Figure 9.17). This earthquake's focal mechanism contained a large component of opening mode displacement (Dreger *et al.*, 2000), and it was followed by upward migration of seismicity over the next several days (Hill *et al.*, 2003). These features of the 1997 activity strongly suggest upward movement of material into a shallow subvertical dike in the caldera's south moat, beginning with the November 22 earthquake. The similarity of the time histories of the water level and strain responses following this earthquake, to those following the 1992 Landers earthquake, leads to the hypothesis that incremental propagation or inflation of dikes can be stimulated at Long Valley by distant earthquakes.

9.5.3 Eruptions of Hekla, Iceland, in 1991 and 2000

A small network of Sacks–Evertson strainmeters was installed in southern Iceland in 1979 with the objective of capturing strain changes associated with an expected moderate earthquake in the south Iceland seismic zone (Figure 9.18). The volcano Hekla is in the study area but had erupted in 1970; from its eruption history, it was not expected to erupt again for at least many decades. Thus, the network was not designed to provide strong constraints on volcanic activity at Hekla; the nearest site (BUR) is 15 km from the volcano and the others are

Figure 9.18. Map of southern Iceland showing the location of the borehole strainmeter network, Hekla Volcano, and south Iceland seismic zone.

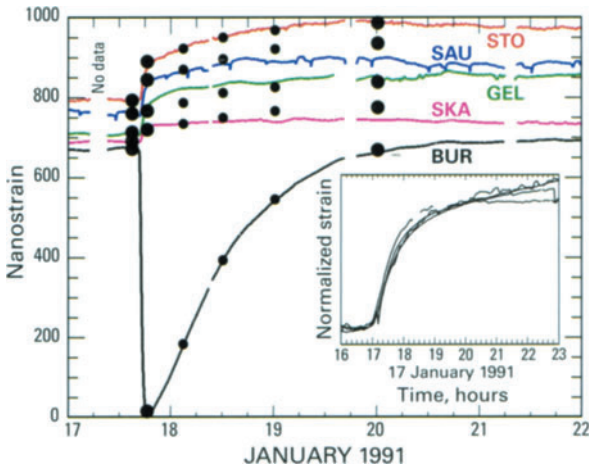

Figure 9.19. Borehole strain data for a 5-day period beginning 1 day prior to the 17 January 1991 eruption of Hekla Volcano, Iceland. Expansion is positive. Earth tides and atmospheric-pressure-induced strain changes have been removed. *Inset* (covering 7 hours, with amplitudes normalized) shows that even the 4 more-distant sites undergo expansion in a remarkably coherent manner. Large solid circles show strain changes calculated from modeling the eruption in two stages. Stage 1 (deflation of a deep reservoir together with dike formation) takes place during the interval from initiation of magma movement until the output from the strainmeter at BUR reaches a minimum. During the following two days (stage 2), when the eruption was essentially complete, the data can be modeled solely by continued deflation of the deep source. Smaller circles show results of calculations for intermediate times during stage 2. These three points correspond to pressure decreases of 30%, 60%, and 80% of the total change of 14 MPa during stage 2 (Linde *et al.*, 1993). All times are local.

at distances of 35–45 km, although they do cover a wide range of azimuths. But the eruption in 1970 apparently marked a change in eruptive nature from infrequent (~100 years) large eruptions to small eruptions every 10 years or so. At the time of the 1980 eruption, only analog chart records of strain were available and these had significant gaps. But the eruptions in 1991 and 2000 were both well recorded on telemetered digital records.

Analysis of the January 1991 eruption was reported by Linde *et al.* (1993). All the more distant strainmeters showed extensional strain changes during the approximately two days during which the eruption was most active (Figure 9.19). However, the nearest station (BUR) drew a more complicated record, with large rapid contraction during the first two hours (Figure 9.20) followed by expansion for the next two days. These changes were modeled in terms of a deflating point spherical pressure source (Mogi source) together with a dike that propagated from a depth of 4 km to the surface (Figure 9.20). The strike and length of the dike were determined from surface observations of the eruption. From an expanded timescale plot (Figure 9.21), it is clear that the strain changes at BUR start about 30 minutes before the eruption. These pre-eruptive changes start with the initiation of dike propagation at depth. Thus, in the case of Hekla, the vertical speed of dike propagation is about $8\,\mathrm{km\,hr^{-1}}$, indicating that the process is driven by gas rather than high-viscosity magma.

The February 2000 eruption of Hekla (Agustsson *et al.*, 2000; Linde and Sacks, 2000) was somewhat smaller than that in 1991, but the strain records were remarkably similar (Figure 9.22), indicating that both eruptions took place with essentially the same geometry. After the 1991 eruption, seismographs were installed closer to Hekla with one station 2 km from the summit. Historically, Hekla has remained seismically quiet except during eruptions. In 2000, the seismograph 2 km from the summit recorded earthquakes at Hekla starting about 90 minutes before the eventual eruption. The alert caused R. Stefansson (chief of the geophysics group at the Iceland Meteorological Office) to come to the office on a Saturday afternoon where he closely monitored the seismic and strain activity. As the earthquake activity increased, he issued an unofficial alert and requested the meteorologists to determine the wind velocity at altitudes of 10 km and above. The strain data are telemetered to the office at 50 samples per second with 20-bit resolution. When Stefansson saw the BUR strain decreasing as in 1991 (Figure 9.23), he issued a formal prediction and warning. This was broadcast to

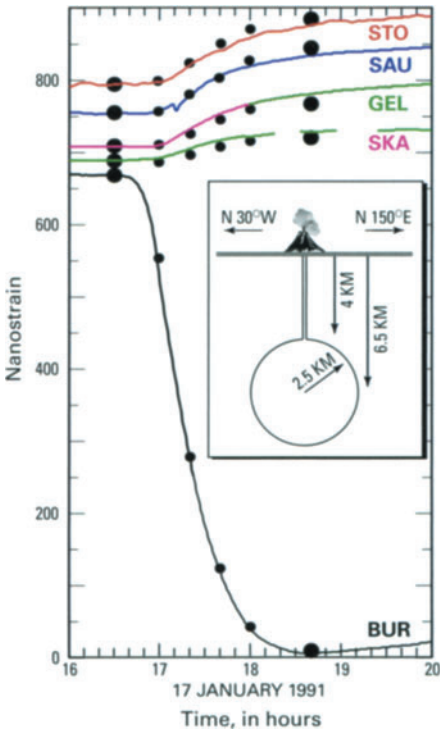

Figure 9.20. Borehole strain data for a 4-hour period that includes the onset of the 1991 eruption of Hekla Volcano. *Inset* shows the model used to calculate points overlaid on the curve. Symbols are the same as Figure 9.19. The exact onset time of the eruption is not known from direct observations owing to inclement weather. However, airport radar observations set the time between 17:00 hr and 17:10 hr (when the plume was already 11.5 km high), and farmers near the volcano reported seeing activity at ~17:05 hr (Linde *et al.*, 1993). All times are local.

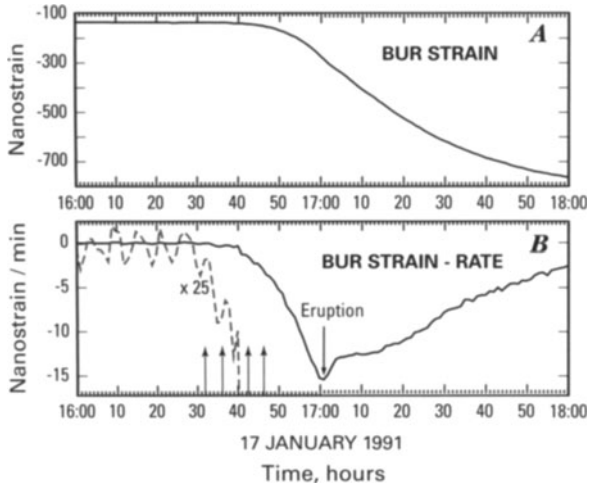

Figure 9.21. Strain data for 2 hours on 17 January 1991 from station BUR (A), and its time derivative (B), on an expanded timescale.

the public and to the Civil Aviation authorities, the latter because Hekla eruptions always send an ash plume to heights greater than 10 km within minutes of the eruption. This successful prediction was possible only because the strain changes are a direct indication of magma movement, and because the eruption repeated the pattern that had been recorded in the 1991 eruption.

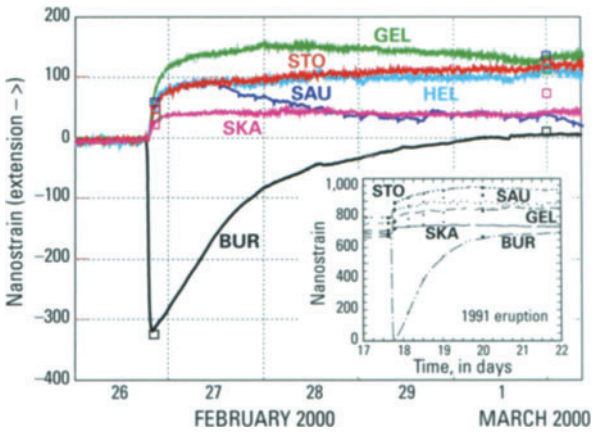

Figure 9.22. Borehole strain data from the February 2000 eruption of Hekla Volcano, together with comparable data from the same five stations for the 1991 eruption (*inset*).

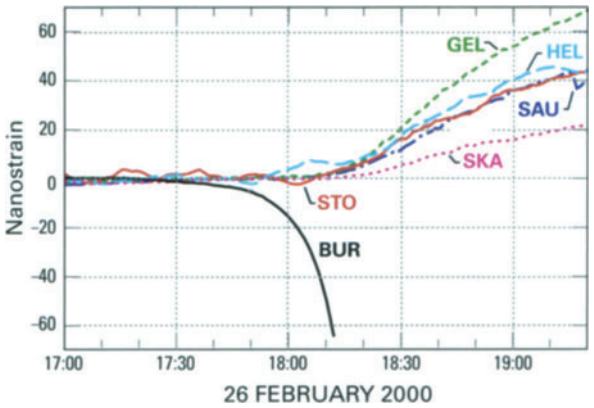

Figure 9.23. Borehole strain data for a 2.5-hour period including the onset of the 2000 eruption of Hekla. Times are local.

9.5.4 Eruption of Usu Volcano, Japan, March 2000

Usu is a dacitic stratovolcano on the island of Hokkaido, Japan, which has been active episodically since the 17th century. During its penultimate eruption in 1977–1978, manual groundwater level measurements were being made in a 370 m deep well 2 km east of the summit (Watanabe, 1983). Following a pumice eruption in December 1977, the water level in this well was found to have risen 37 m relative to 1972 measurements. Following this finding, more frequent measurements of water level showed it to be falling steeply, with some small rises, especially accompanying felt earthquakes.

Usu volcano erupted again on 31 March 2000. Prior to this most recent eruption, a number of CGPS stations had been installed around the volcano. Groundwater levels in a number of wells were also being recorded, some specifically for the purpose of detecting crustal deformation, and others to monitor conditions in the area's geothermal aquifers.

Shibata and Akita (2001) report large changes in groundwater level preceding the eruption. They observed decreasing groundwater levels beginning as early as six months prior to the eruption, which they attributed to an increase of cracking near the surface induced by an influx of magma into the subvolcanic fracture system. Matsumoto *et al.* (2002) reported water level increases shortly before the eruption in slightly more distant wells. Three days after the eruption began, the water level in one well suddenly increased and began to spout, representing a fluid pressure increase of more than 1 MPa, possibly due to the addition of thermal fluid through new cracks created during the eruption.

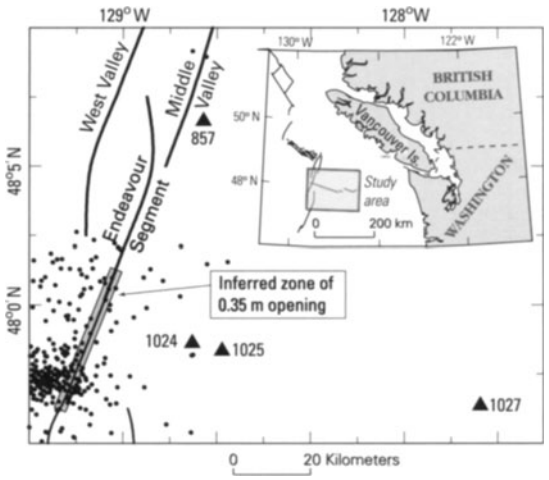

Figure 9.24. Map showing the location of CORK borehole observatory sites (triangles), the Endeavour segment of the Juan de Fuca Ridge, and the inferred surface projection of a spreading event (modified from Davis *et al.*, 2001). Dots represent earthquakes recorded using the US Navy SOSUS array for the period 7 June–17 July 1999 (from NOAA/Pacific Marine Environmental Laboratory, Newport, Oregon).

9.5.5 Spreading of the western Pacific sea floor on the Juan de Fuca Ridge

Davis *et al.* (2001) describe 4 years of hourly fluid pressure data measured in subsea boreholes penetrating young (<3.6 Ma) oceanic crust near the axis and on the eastern flank of the Juan de Fuca Ridge, offshore the northwestern coast of North America (Figure 9.24). The boreholes are open to permeable basalts overlain by as much as several hundred meters of relatively impermeable sediments, so that confined conditions prevail at the depths where fluid pressure is being monitored. Fluid pressure records from these subsea boreholes contain fluctuations caused by tidal changes in the load of the overlying ocean (about 2.6 km deep), changes in atmospheric pressure, and other changes in ocean loading due to fluid circulation patterns. As for pressure records from continental boreholes, these effects can be removed using linear regression and harmonic analysis to reveal smaller signals and to constrain the ratio of fluid pressure change to crustal strain.

In 1999, a seismic swarm initiated on 8 June with a M 2.8 earthquake. The swarm included 8 events with magnitudes up to 4.1 detected by onshore seismic networks, and several hundred events detected by the US Navy SOSUS array. In three boreholes, 25 to 101 km from the ridge axis, fluid pressure rises of 0.1–1.6 KPa (1–16 cm of water) occurred abruptly with the first event and then continued more gradually over the succeeding hours to days, with similar time histories but time scales lengthening with increasing distance from the ridge (Figure 9.25). Davis *et al.* (2001) estimated strain sensitivities of 0.3–0.4 m per microstrain for these boreholes, based on physical properties of the formation and tidal response, and inferred initial strains of 0.5 microstrain contraction at the nearest site and 0.024 microstrain contraction at the most distant site. These strains are far larger than can be accounted for by any earthquakes in the swarm. Davis *et al.* (2001) modeled the observed strains with 0.35 m of opening perpendicular to the ridge, extending from the surface to a depth of 3 km and approximately 40 km along the strike of the ridge.

The longer rise times for the fluid pressure disturbances at increasing distances from the ridge axis would not be expected if the fluid pressure changes were simply proportional to poroelastic strain; in such case, all sensors would have the same time history as the strain imposed by the spreading event. Instead, Davis *et al.* (2001) showed that the time histories of the fluid pressure changes are well matched by assuming 1-D diffusion of the fluid pressure pulse induced by the spreading event. This observation illustrates an important difference between the observations made by a strainmeter and those made by a fluid pressure sensor. In this case, the fluid pressure records do not tightly constrain the

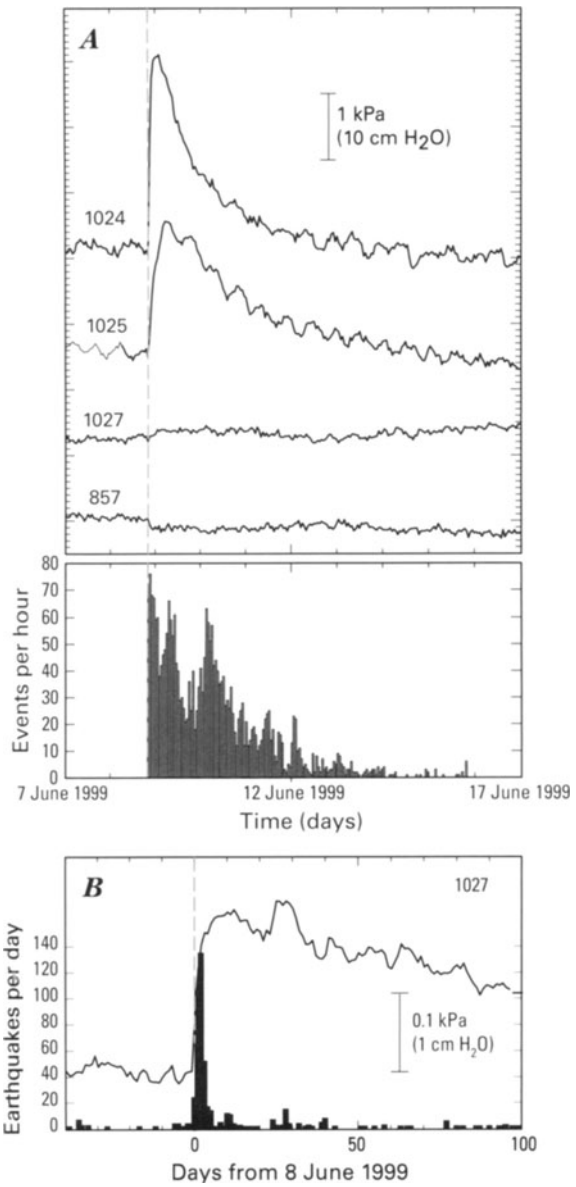

Figure 9.25. (A) Formation pressure for the 10-day period 7 June–17 June 1999 from sites 1024, 1025, 1027, and 857 with responses to tidal, barometric, and oceanographic loading removed, and number of earthquakes per hour. (B) Expanded-scale 140-day record of formation pressure from site 1027 (tidal, barometric, and oceanographic loading removed), with number of earthquakes per day. Pressure data from Davis *et al.* (2001); seismicity from NOAA/Pacific Marine Environmental Laboratory, Newport, Oregon.

detailed time history of the spreading event. Nevertheless, the results are remarkable in that a fluid pressure change of 2 cm of water, with a rise time of about 10 days, was clearly detected at site 1027, 100 km from the source (Figure 9.25). Moreover, the strain causing the fluid pressure change could be quantified, and the data clearly show crustal deformation beyond that represented by the earthquakes themselves, strongly implying the occurrence of a spreading event.

9.6 SUMMARY

Borehole strainmeters and groundwater level sensors in wells are increasingly being deployed near active volcanoes, and the examples described here demonstrate the promise of these techniques for enhancing predictive capabilities and learning about volcanic processes at depth. Noise is reduced by observing in a borehole environment. The resulting capacity to detect small signals promotes safety through automatic operation and installation at greater distances from volcanic vents. Moreover, signals originating from deep magma movements can be detected, and datasets that continue through the eruption can be obtained. The detailed time histories of deformation permit the ascent of magma to be tracked continuously in time.

Borehole strainmeter and fluid pressure monitoring installations can have somewhat greater initial costs than other geodetic techniques. A borehole must be available, and usually must be specially drilled if a strainmeter is to be installed. The first several months of strainmeter data may not be useful, due to grout curing, borehole creep, and instrument adjustments. For groundwater level data, it is also desirable to record data for a long enough period to determine the usual responses to precipitation and climate, prior to attempting interpretation in terms of crustal strain. For these reasons, these techniques are only useful in a volcanic crisis response if the instruments have been deployed at least several months ahead of time.

Borehole-strain measurements are most useful when made within a network of geodetic stations where absolute crustal movements also can be determined. When deployed well ahead of an eruption as part of an integrated volcano-monitoring network, crustal strain measurements in boreholes provide invaluable information about volcanic processes, and have already been used to issue a public warning in advance of an eruption.